2019 American Control Conference (ACC)
Philadelphia, PA, USA, July 10-12, 2019

Relative Moving Target Tracking and Circumnavigation

Jerel Nielsen[1] and Randal Beard[2]

Abstract— **This paper develops observers and controllers for relative estimation and circumnavigation of a moving ground target using bearing-only measurements or range with bearing measurements. A bearing-only observer, range with bearing observer, a general circumnavigation velocity command for an arbitrary aircraft, and nonlinear velocity-based multirotor controller are developed. The observers are designed in the body-fixed reference frame, while the velocity command and multirotor controller are developed in the body-level frame, independent of aircraft heading. This enables target circumnavigation in GPS-denied environments when only a camera-IMU estimator is used for state estimation and ensures observable conditions for the estimator. Simulation results demonstrate the effectiveness of the observers, velocity command, and multirotor controller under various target motions.**

I. Nomenclature

R_a^b	Rotation from reference frame a to b
$\hat{a}$	Estimate of true variable a
$\bar{a}$	Measurement of a
$\dot{a}$	Time derivative a

Superscript

i	Expressed in the inertial coordinate frame
l	Expressed in the aircraft's body-level coordinate frame
b	Expressed in the aircraft's body coordinate frame
$\top$	Matrix transpose

Subscript

a/b	The state of frame a w.r.t. frame b (e.g. position or velocity)

The skew symmetric operator is defined by $\cdot^\wedge$, such that $\mathbf{a}^\wedge\mathbf{b} = \mathbf{a} \times \mathbf{b}$. We also make use the basis vectors

$$\mathbf{e}_1 = \begin{bmatrix}1 & 0 & 0\end{bmatrix}^\top \tag{1}$$

$$\mathbf{e}_2 = \begin{bmatrix}0 & 1 & 0\end{bmatrix}^\top \tag{2}$$

$$\mathbf{e}_3 = \begin{bmatrix}0 & 0 & 1\end{bmatrix}^\top, \tag{3}$$

and denote other unit vectors by $\mathbf{e}_*$.

*This research was supported through the U.S. Department of Defense SMART Scholarship program and by the Center for Unmanned Aircraft Systems (C-UAS), a National Science Foundation-sponsored industry/university cooperative research center (I/UCRC) under NSF Award No. IIP-1650547 along with significant contributions from C-UAS industry members, and in part by AFRL grant FA8651-13-1-0005.

[1]Jerel Nielsen is a graduate student in the Electrical and Computer Engineering department at Brigham Young University, Provo, UT 84602, USA jerel.nielsen@gmail.com

[2]Randal Beard is a professor of the Electrical and Computer Engineering department at Brigham Young University, Provo, UT 84602, USA beard@byu.edu

II. Introduction

Target tracking and surveillance from an unmanned air vehicle (UAV) has been an area of interest in the research community for many years, primarily aimed at military applications, due to the cost sensors and aerial platforms. In recent years however, the development and proliferation of increasingly smaller sensors, such as inertial measurement units (IMU) and video cameras has caused the emergence of small unmanned air systems (sUAS). This phenomenon has greatly multiplied the possibilities for aerial target tracking and brought forth many works related to the circumnavigation of targets [1], [2], [3], [4], [5], [6], [7].

In addition to the interest in target circumnavigation brought on by the multiplicity of sUAS, a significant effort has been put forth to fuse IMU measurements with camera measurements. The IMU provides high rate measurements of linear acceleration and angular rate, while the camera provides direction or full vector measurements to landmarks, depending on the type of camera. These types of measurements are ideal for continuous-discrete Kalman filtering because the mechanization of IMU measurements provides high rate prediction, while the camera provides low rate corrections. The fusion of these measurements has been thoroughly demonstrated through Kalman filtering, optimization, and nonlinear techniques in many recent visual-inertial odometry (VIO) and simultaneous localization and mapping (SLAM) works [8], [9], [10], [11], [12], [13].

Many of the existing circumnavigation algorithms assume a known inertial state [1], [5]. These will not perform as well when the following agent is only equipped with a camera and IMU for state estimation because the global position and heading are not observable [14]. Others have developed algorithms for GPS-denied target tracking and following [3], [15] with successful hardware demonstrations. Some even follow targets using image-based visual servoing (IBVS) techniques [16]. However, these assume a known object size or appearance and do not address the observability required for the state estimator to estimate IMU biases, enabling accurate attitude estimation.

This paper develops observers and controllers for relative estimation and circumnavigation of a moving ground target, assuming that the aircraft is equipped with only a camera and IMU for state estimation. While cameras typically provide only bearing information, some modern cameras are capable of providing depth information. When a depth measurement is not available, we can create pseudo-depth measurements by approximating target position relative to static landmark position estimates [17]. Therefore, we develop two observers

978-1-5386-7926-5/$31.00 ©2019 AACC

in this paper, where the first uses bearing-only information and the second takes advantage of full vector information. Following the target observers, we also use nonlinear system theory to define a commanded velocity vector to drive the aircraft to a circumnavigating path about the target. Finally, a nonlinear controller for a multirotor aircraft is derived in the body-level reference frame to drive the multirotor to a commanded velocity. While we do not develop multirotor state estimator in this paper, we note that observability of the IMU biases is also guaranteed because of the persistent excitation of landmark bearing measurements [18] resulting from the circumnavigating motion.

We begin in Section III by developing the target observers using bearing-only and range with bearing measurements. This is followed by Section IV-A, where we derive the commanded body-level velocity needed to bring an arbitrary aircraft to a desired radius and altitude relative to the target. Next in Section IV-B, we design a controller specific to a multirotor aircraft to drive the multirotor's velocity to a commanded body-level velocity. Lastly, Section V demonstrates the effectiveness of these observers and controllers under various target motions and discusses the results.

III. Target Estimation

A. Bearing-only Measurements

The position of the target relative to the UAS and its time derivative are given by

$$\mathbf{p}^b_{t/b} = R^b_i \left(\mathbf{p}^i_{t/i} - \mathbf{p}^i_{b/i} \right) \tag{4}$$

$$\dot{\mathbf{p}}^b_{t/b} = \dot{R}^b_i \left(\mathbf{p}^i_{t/i} - \mathbf{p}^i_{b/i} \right) + R^b_i \left(\dot{\mathbf{p}}^i_{t/i} - \dot{\mathbf{p}}^i_{b/i} \right). \tag{5}$$

Assuming a stationary target $\dot{\mathbf{p}}^i_{t/i} = 0$ and inserting $\dot{R}^b_i = -\left(\boldsymbol{\omega}^b_{b/i}\right)^\wedge R^b_i$, this becomes

$$\dot{\mathbf{p}}^b_{t/b} = -\boldsymbol{\omega}^b_{b/i} \times \mathbf{p}^b_{t/b} - \mathbf{v}^b_{b/i}, \tag{6}$$

where $\boldsymbol{\omega}^b_{b/i}$ and $\mathbf{v}^b_{b/i}$ are the angular and linear rates of the UAS. Here, we have assumed that the aircraft's visual-inertial estimator is working well, such that its observable states are known, and we have also assumed a stationary target. However, the error will remain bounded for slowly moving targets as shown in [5].

Proposition 1: Assuming that the camera only measures target direction $\mathbf{e}_t = \frac{\mathbf{p}^b_{t/b}}{\left\|\mathbf{p}^b_{t/b}\right\|}$, an observer for relative target position may be given by

$$\dot{\hat{\mathbf{p}}}^b_{t/b} = -\boldsymbol{\omega}^b_{b/i} \times \hat{\mathbf{p}}^b_{t/b} - \mathbf{v}^b_{b/i} - k_1 \left(I - \mathbf{e}_t \mathbf{e}_t^\top \right) \hat{\mathbf{p}}^b_{t/b}, \tag{7}$$

where k_1 is a positive gain.

Proof: With the error $\tilde{\mathbf{p}}^b_{t/b} = \hat{\mathbf{p}}^b_{t/b} - \mathbf{p}^b_{t/b}$, error kinematics are given by

$$\dot{\tilde{\mathbf{p}}}^b_{t/b} = \left(-\left(\boldsymbol{\omega}^b_{b/i}\right)^\wedge - k_1 \left(I - \mathbf{e}_t \mathbf{e}_t^\top \right) \right) \tilde{\mathbf{p}}^b_{t/b}. \tag{8}$$

Now, define the Lyapunov function candidate $\mathcal{L} = \frac{1}{2} \left(\tilde{\mathbf{p}}^b_{t/b} \right)^\top \tilde{\mathbf{p}}^b_{t/b}$ and differentiate to obtain

$$\dot{\mathcal{L}} = -k_1 \left\| \tilde{\mathbf{p}}^b_{t/b} \right\|^2 + k_1 \left(\mathbf{e}_t^\top \tilde{\mathbf{p}}^b_{t/b} \right)^2, \tag{9}$$

which is negative semi-definite by the Cauchy-Schwarz inequality

$$\left| \left\langle \mathbf{e}_t, \tilde{\mathbf{p}}^b_{t/b} \right\rangle \right| \leq \|\mathbf{e}_t\| \left\| \tilde{\mathbf{p}}^b_{t/b} \right\| = \left\| \tilde{\mathbf{p}}^b_{t/b} \right\|. \tag{10}$$

Furthermore, the set $S = \left\{ \left(\mathbf{e}_t, \tilde{\mathbf{p}}^b_{t/b} \right) \middle| \dot{\mathcal{L}} \left(\mathbf{e}_t, \tilde{\mathbf{p}}^b_{t/b} \right) = 0 \right\}$ contains only trajectories, where $\tilde{\mathbf{p}}^b_{t/b} = 0$ or the directions of $\mathbf{e}_t$ and $\hat{\mathbf{p}}^b_{t/b}$ are aligned. Suppose that we begin with a trajectory where these directions are aligned but $\tilde{\mathbf{p}}^b_{t/b} \neq 0$. We then have the relationship $\mathbf{e}_t \times \tilde{\mathbf{p}}^b_{t/b} = \frac{d}{dt} \left[\mathbf{e}_t \times \tilde{\mathbf{p}}^b_{t/b} \right] = 0$, and evaluating the time derivative yields $\dot{\mathbf{e}}_t \times \tilde{\mathbf{p}}^b_{t/b} + \mathbf{e}_t \times \dot{\tilde{\mathbf{p}}}^b_{t/b} = 0$, where $\dot{\mathbf{e}}_t = -\boldsymbol{\omega}^b_{b/i} \times \mathbf{e}_t - \left(I - \mathbf{e}_t \mathbf{e}_t^\top \right) \frac{\mathbf{v}^b_{b/i}}{\left\| \mathbf{p}^b_{t/b} \right\|}$. Because $\mathbf{e}_t \times \tilde{\mathbf{p}}^b_{t/b} = 0$, its time derivative simplifies to $\mathbf{v}^b_{b/i} \times \tilde{\mathbf{p}}^b_{t/b} = 0$. The alignment of $\mathbf{e}_t$ and $\hat{\mathbf{p}}^b_{t/b}$ implies alignment of $\mathbf{e}_t$ and $\tilde{\mathbf{p}}^b_{t/b}$. Therefore when $\mathbf{v}^b_{b/i}$ is not aligned with $\mathbf{e}_t$, we have $\mathbf{v}^b_{b/i} \times \tilde{\mathbf{p}}^b_{t/b} \neq 0$. Thus, the trajectory will leave the set S, except when $\tilde{\mathbf{p}}^b_{t/b} = 0$ or when $\mathbf{v}^b_{b/i}$ is aligned with $\mathbf{e}_t$.

B. Range with Bearing Measurements

The position and velocity of the target relative to the agent are given by

$$\mathbf{p}^b_{t/b} = R^b_i \left(\mathbf{p}^i_{t/i} - \mathbf{p}^i_{b/i} \right) \tag{11}$$

$$\mathbf{v}^b_{t/b} = R^b_i \left(\mathbf{v}^i_{t/i} - \mathbf{v}^i_{b/i} \right). \tag{12}$$

Assuming a constant velocity target $\dot{\mathbf{v}}^i_{t/i} = 0$ and inserting $\dot{R}^b_i = -\left(\boldsymbol{\omega}^b_{b/i}\right)^\wedge R^b_i$, this becomes

$$\dot{\mathbf{p}}^b_{t/b} = \mathbf{v}^b_{t/b} - \boldsymbol{\omega}^b_{b/i} \times \mathbf{p}^b_{t/b} \tag{13}$$

$$\dot{\mathbf{v}}^b_{t/b} = -\boldsymbol{\omega}^b_{b/i} \times \mathbf{v}^b_{t/b} - \dot{\mathbf{v}}^b_{b/i}, \tag{14}$$

where the aircraft's acceleration $\dot{\mathbf{v}}^b_{b/i}$ is measured by its IMU. This may be written in terms of the accelerometer measurement as

$$\dot{\mathbf{v}}^b_{b/i} = \bar{\mathbf{a}}^b_{b/i} + g R^b_l \mathbf{e}_3 - \boldsymbol{\omega}^b_{b/i} \times \mathbf{v}^b_{b/i}, \tag{15}$$

where g is gravity's magnitude and $\bar{\mathbf{a}}^b_{b/i}$ is the measured acceleration of the IMU.

Proposition 2: Assuming that the camera measures relative target position $\mathbf{p}^b_{t/b}$ via RGB-D camera or pseudo-depth, an observer may be given by

$$\dot{\hat{\mathbf{p}}}^b_{t/b} = \hat{\mathbf{v}}^b_{t/b} - \boldsymbol{\omega}^b_{b/i} \times \hat{\mathbf{p}}^b_{t/b} - k_1 \tilde{\mathbf{p}}^b_{t/b} \tag{16}$$

$$\dot{\hat{\mathbf{v}}}^b_{t/b} = -\boldsymbol{\omega}^b_{b/i} \times \hat{\mathbf{v}}^b_{t/b} - \dot{\mathbf{v}}^b_{b/i} - k_2 \tilde{\mathbf{p}}^b_{t/b}, \tag{17}$$

where k_1 and k_2 are a positive gains.

Proof: With the errors $\tilde{\mathbf{p}}^b_{t/b} = \hat{\mathbf{p}}^b_{t/b} - \mathbf{p}^b_{t/b}$ and $\tilde{\mathbf{v}}^b_{t/b} = \hat{\mathbf{v}}^b_{t/b} - \mathbf{v}^b_{t/b}$, error kinematics are given by

$$\dot{\tilde{\mathbf{p}}}^b_{t/b} = -\boldsymbol{\omega}^b_{b/i} \times \tilde{\mathbf{p}}^b_{t/b} + \tilde{\mathbf{v}}^b_{t/b} - k_1 \tilde{\mathbf{p}}^b_{t/b} \tag{18}$$

$$\dot{\tilde{\mathbf{v}}}^b_{t/b} = -\boldsymbol{\omega}^b_{b/i} \times \tilde{\mathbf{v}}^b_{t/b} - k_2 \tilde{\mathbf{p}}^b_{t/b}. \tag{19}$$

Now, define the Lyapunov function candidate $\mathcal{L} = \frac{1}{2}\left(\left(\tilde{\mathbf{p}}^b_{t/b}\right)^\top \tilde{\mathbf{p}}^b_{t/b} + \frac{1}{k_2}\left(\tilde{\mathbf{v}}^b_{t/b}\right)^\top \tilde{\mathbf{v}}^b_{t/b}\right)$ and differentiate to obtain

$$\dot{\mathcal{L}} = -k_z \left\|\tilde{\mathbf{p}}^b_{t/b}\right\|^2, \tag{20}$$

which is negative semi-definite.

Moreover, the set $S = \left\{\left(\tilde{\mathbf{p}}^b_{t/b}, \tilde{\mathbf{v}}^b_{t/b}\right) \middle| \dot{\mathcal{L}}\left(\tilde{\mathbf{p}}^b_{t/b}, \tilde{\mathbf{v}}^b_{t/b}\right) = 0\right\}$ contains only trajectories, where $\tilde{\mathbf{p}}^b_{t/b} = 0$. Suppose that we begin with a trajectory with $\tilde{\mathbf{p}}^b_{t/b} = 0$ and $\tilde{\mathbf{v}}^b_{t/b} \neq 0$. Under this condition, the errors evolve according to

$$\dot{\tilde{\mathbf{p}}}^b_{t/b} = \tilde{\mathbf{v}}^b_{t/b} \tag{21}$$

$$\dot{\tilde{\mathbf{v}}}^b_{t/b} = -\boldsymbol{\omega}^b_{b/i} \times \tilde{\mathbf{v}}^b_{t/b}, \tag{22}$$

indicating that this trajectory will leave the set S, except when $\tilde{\mathbf{p}}^b_{t/b} = \tilde{\mathbf{v}}^b_{t/b} = 0$.

■

IV. Circumnavigation

We derive the following velocity and multirotor controllers in the body-level reference frame to remove any dependence on heading.

A. Velocity Control

In this section, we derive the commanded velocity in the body-level reference frame needed to bring an arbitrary aircraft to a circumnavigating orbit about a target at some constant, desired relative radius r_d and altitude h_d. The relative radius and altitude in the body-level frame are computed by rotating the body-fixed relative target position into the body-level frame and projecting onto the horizontal plane and vertical axis. These are written in terms of the relative target position by

$$r = \left\|\left(I - \mathbf{e}_3\mathbf{e}_3^\top\right) R^l_b \mathbf{p}^b_{t/b}\right\| \tag{23}$$

$$h = \mathbf{e}_3^\top R^l_b \mathbf{p}^b_{t/b}. \tag{24}$$

Differentiating these w.r.t. time yields

$$\dot{r} = \mathbf{e}_r^\top \left(\mathbf{v}^l_{t/i} - \mathbf{v}^l_{b/i}\right) \tag{25}$$

$$\dot{h} = \mathbf{e}_3^\top \left(\mathbf{v}^l_{t/i} - \mathbf{v}^l_{b/i}\right), \tag{26}$$

where $\mathbf{e}_r$ is the horizontal target direction in the body-level frame and $\mathbf{e}_r \perp \mathbf{e}_3$. Writing $\mathbf{e}_r$ in terms of $\mathbf{e}_t$, we also have

$$\mathbf{e}_r = \frac{\left(I - \mathbf{e}_3\mathbf{e}_3^\top\right) R^l_b \mathbf{e}_t}{\left\|\left(I - \mathbf{e}_3\mathbf{e}_3^\top\right) R^l_b \mathbf{e}_t\right\|}. \tag{27}$$

Proposition 3: Define the errors $\tilde{r} = r - r_d$, $\tilde{h} = h - h_d$, and let the commanded velocity in the body-level frame be given by

$$\mathbf{v}^l_c = k_r \tilde{r}\mathbf{e}_r + v_t \frac{\mathbf{e}_3 \times \mathbf{e}_r}{\|\mathbf{e}_3 \times \mathbf{e}_r\|} + k_h \tilde{h}\mathbf{e}_3 + R^l_b \hat{\mathbf{v}}^b_{t/i}, \tag{28}$$

where k_r and k_h are positive gains and v_t is the tangential velocity chosen by the user. Note that for bearing-only target estimation $\hat{\mathbf{v}}^b_{t/i} = 0$ and for range with bearing target estimation $\hat{\mathbf{v}}^b_{t/i} = \hat{\mathbf{v}}^b_{t/b} + \hat{\mathbf{v}}^b_{b/i}$.

Proof: Differentiating the relative radial and altitude errors with respect to time, we obtain

$$\dot{\tilde{r}} = \mathbf{e}_r^\top \left(\mathbf{v}^l_{t/i} - \mathbf{v}^l_{b/i}\right) \tag{29}$$

$$\dot{\tilde{h}} = \mathbf{e}_3^\top \left(\mathbf{v}^l_{t/i} - \mathbf{v}^l_{b/i}\right). \tag{30}$$

Selecting $\mathbf{v}^l_{b/i} = \mathbf{v}^l_c$ from (28), these become

$$\dot{\tilde{r}} = -k_r \tilde{r} \tag{31}$$

$$\dot{\tilde{h}} = -k_h \tilde{h}, \tag{32}$$

ensuring that $\tilde{r} \to 0$ and $\tilde{h} \to 0$.

When the target velocity estimate is fixed at zero, as is the case for bearing-only estimation, the Lyapunov function candidate $\mathcal{L} = \frac{1}{2}\left(\tilde{r}^2 + \tilde{h}^2\right)$ has the time derivative

$$\dot{\mathcal{L}} = -k_r \tilde{r}^2 - k_h \tilde{h}^2 + \left(\tilde{r}\mathbf{e}_r^\top + \tilde{h}\mathbf{e}_3^\top\right) \mathbf{v}^l_{t/i}. \tag{33}$$

Define $\mathbf{x} = \begin{bmatrix}\tilde{r} & \tilde{h}\end{bmatrix}^\top$ and (33) becomes

$$\dot{\mathcal{L}} = -\mathbf{x}^\top A \mathbf{x} + \mathbf{b}^\top \mathbf{x}, \tag{34}$$

where

$$A = \begin{bmatrix} k_r & 0 \\ 0 & k_h \end{bmatrix} \tag{35}$$

$$\mathbf{b} = \begin{bmatrix} \mathbf{e}_r^\top \mathbf{v}^l_{t/i} \\ \mathbf{e}_3^\top \mathbf{v}^l_{t/i} \end{bmatrix}. \tag{36}$$

With $\sigma_{min} = \min(k_r, k_h)$ and $\sigma_{max} = \max(k_r, k_h)$, we then have

$$\sigma_{min} \|\mathbf{x}\|^2 \leq \mathbf{x}^\top A \mathbf{x} \leq \sigma_{max} \|\mathbf{x}\|^2, \tag{37}$$

which yields the relation

$$\dot{\mathcal{L}} \leq \sigma_{min} \|\mathbf{x}\| \left(\frac{\|\mathbf{b}\|}{\sigma_{min}} - \|\mathbf{x}\|\right). \tag{38}$$

Therefore, $\dot{\mathcal{L}} < 0$ if $\|\mathbf{x}\| > \frac{\|\mathbf{b}\|}{\sigma_{min}}$ and the solution is ultimately bounded in finite time. After convergence to the bounded region, we have

$$\|\mathbf{x}\| \leq \frac{\|\mathbf{b}\|}{\sigma_{min}}, \tag{39}$$

which depends on target velocity but can be made arbitrarily small by choosing k_r, k_h to be arbitrarily large.

■

We note that in practice, the UAS is constrained by its own maximum velocity, so there exists a limit to the effect of these gains.

To reduce the likelihood of the target moving out of the camera's field of view, the desired radius and altitude may be chosen according to the direction of the camera optical axis during level flight. For a known optical axis angle from vertical θ, we may choose a desired relative altitude and let the desired radius be chosen mathematically to align the level optical axis with the target by

$$r_d = h_d \tan\theta. \tag{40}$$

B. Multirotor Velocity Control

Neglecting wind and drag, velocity dynamics of a multirotor aircraft in the body-level frame are given by

$$\dot{\mathbf{v}}^l_{b/i} = g\mathbf{e}_3 - \frac{T}{m}R^l_b\mathbf{e}_3 - \boldsymbol{\omega}^l_{l/i} \times \mathbf{v}^l_{b/i}, \tag{41}$$

where g gravitational magnitude, T is thrust, m is vehicle mass, and the yaw rate of the body-level frame is

$$\boldsymbol{\omega}^l_{l/i} = \mathbf{e}_3\mathbf{e}_3^\top R^l_b\boldsymbol{\omega}^b_{b/i}. \tag{42}$$

Assuming a known hover throttle signal s_h, we approximate thrust with $T \approx mg\frac{s}{s_h}$ and (41) becomes

$$\dot{\mathbf{v}}^l_{b/i} = g\left(I - \frac{s}{s_h}R^l_b\right)\mathbf{e}_3 - \boldsymbol{\omega}^l_{l/i} \times \mathbf{v}^l_{b/i}. \tag{43}$$

Defining the velocity error $\tilde{\mathbf{v}} = \mathbf{v}^l_c - \mathbf{v}^l_{b/i}$ and holding the command constant, the time derivative is given by

$$\dot{\tilde{\mathbf{v}}} = -g\left(I - \frac{s}{s_h}R^l_b\right)\mathbf{e}_3 + \boldsymbol{\omega}^l_{l/i} \times \mathbf{v}^l_{b/i}. \tag{44}$$

Now, let

$$\mathbf{u} = sR^l_b\mathbf{e}_3, \tag{45}$$

and (44) becomes

$$\dot{\tilde{\mathbf{v}}} = \frac{g}{s_h}\mathbf{u} - g\mathbf{e}_3 + \boldsymbol{\omega}^l_{l/i} \times \mathbf{v}^l_{b/i}. \tag{46}$$

This allows us to select $\mathbf{u}$ as a vector input that drives the velocity error to zero. Define the Lyapunov function candidate $\mathcal{L} = \frac{1}{2}\tilde{\mathbf{v}}^\top\tilde{\mathbf{v}}$ and differentiate to obtain

$$\dot{\mathcal{L}} = \tilde{\mathbf{v}}^\top\left(\frac{g}{s_h}\mathbf{u} - g\mathbf{e}_3 + \boldsymbol{\omega}^l_{l/i} \times \mathbf{v}^l_{b/i}\right). \tag{47}$$

Choose

$$\mathbf{u} = s_h\left(\mathbf{e}_3 - \frac{1}{g}\left(\boldsymbol{\omega}^l_{l/i} \times \mathbf{v}^l_{b/i} + K_v\tilde{\mathbf{v}}\right)\right), \tag{48}$$

and (47) reduces to

$$\dot{\mathcal{L}} = -\tilde{\mathbf{v}}^\top K_v\tilde{\mathbf{v}}, \tag{49}$$

which is negative definite for positive definite K_v. Equating (45) and (48) gives

$$sR^l_b\mathbf{e}_3 = s_h\left(\mathbf{e}_3 - \frac{1}{g}\left(\boldsymbol{\omega}^l_{l/i} \times \mathbf{v}^l_{b/i} + K_v\tilde{\mathbf{v}}\right)\right). \tag{50}$$

Using the current aircraft attitude estimate and solving for the commanded thrust signal yields

$$s_c = s_h\mathbf{e}_3^\top\left(R^l_b\right)^\top\left(\mathbf{e}_3 - \frac{1}{g}\left(\boldsymbol{\omega}^l_{l/i} \times \mathbf{v}^l_{b/i} + K_v\tilde{\mathbf{v}}\right)\right). \tag{51}$$

Now using the commanded thrust signal, we need to solve for the commanded attitude. Substituting $s = s_c$, $R^l_b = \left(R^l_b\right)_c$ in (50) and dividing by s_c, we have

$$\left(R^l_b\right)_c\mathbf{e}_3 = \frac{s_h}{s_c}\left(\mathbf{e}_3 - \frac{1}{g}\left(\boldsymbol{\omega}^l_{l/i} \times \mathbf{v}^l_{b/i} + K_v\tilde{\mathbf{v}}\right)\right). \tag{52}$$

We cannot directly solve for $\left(R^l_b\right)_c$, but this equation tells us that the commanded body-down axis in the body-level frame should point in the direction

$$\left(\mathbf{e}^b_3\right)_c = \frac{\mathbf{e}_3 - \frac{1}{g}\left(\boldsymbol{\omega}^l_{l/i} \times \mathbf{v}^l_{b/i} + K_v\tilde{\mathbf{v}}\right)}{\left\|\mathbf{e}_3 - \frac{1}{g}\left(\boldsymbol{\omega}^l_{l/i} \times \mathbf{v}^l_{b/i} + K_v\tilde{\mathbf{v}}\right)\right\|}. \tag{53}$$

Having the body-down axis pointed in this direction relative to the body-level frame will drive the multirotor to the commanded velocity, regardless of its heading. The commanded body-forward and body-right axes in the body-level frame may then be given by

$$\left(\mathbf{e}^b_2\right)_c = \frac{\left(\mathbf{e}^b_3\right)_c \times \mathbf{e}_1}{\left\|\left(\mathbf{e}^b_3\right)_c \times \mathbf{e}_1\right\|} \tag{54}$$

$$\left(\mathbf{e}^b_1\right)_c = \left(\mathbf{e}^b_2\right)_c \times \left(\mathbf{e}^b_3\right)_c, \tag{55}$$

and the commanded attitude is now given by

$$\left(R^l_b\right)_c = \left[\left(\mathbf{e}^b_1\right)_c \quad \left(\mathbf{e}^b_2\right)_c \quad \left(\mathbf{e}^b_3\right)_c\right]. \tag{56}$$

However, many flight controllers require roll and pitch angles along with a commanded yaw rate. Roll and pitch angles are easily computed from $\left(R^l_b\right)_c$ because it has the form

$$\left(R^l_b\right)_c = \begin{bmatrix} \cos\theta & \sin\phi\sin\theta & \cos\phi\sin\theta \\ 0 & \cos\phi & -\sin\phi \\ -\sin\theta & \sin\phi\cos\theta & \cos\phi\cos\theta \end{bmatrix}, \tag{57}$$

which leads to the commanded roll and pitch angles

$$\phi_c = \tan^{-1}\left(-\frac{\mathbf{e}_2^\top\left(R^l_b\right)_c\mathbf{e}_3}{\mathbf{e}_2^\top\left(R^l_b\right)_c\mathbf{e}_2}\right) \tag{58}$$

$$\theta_c = \tan^{-1}\left(-\frac{\mathbf{e}_3^\top\left(R^l_b\right)_c\mathbf{e}_1}{\mathbf{e}_1^\top\left(R^l_b\right)_c\mathbf{e}_1}\right). \tag{59}$$

Commanded yaw rate can be given by the angular difference about the body z axis between the camera optical axis and the target direction vector. Given the fixed optical axis defined in the multirotor's body reference frame $\mathbf{e}^b_{opt}$, the commanded body yaw rate is given by

$$r_c = k_r\mathbf{e}_3^\top\left(\mathbf{e}^b_{opt} \times \mathbf{e}_t\right), \tag{60}$$

where k_r is a positive gain. This does not drive the angular error in yaw exactly to zero but a high gain can reduce the error close to zero.

V. Simulation Results

To demonstrate the performance of the observers and controllers derived in Sections III and IV, we designed a simulation of a multirotor and a nonholonomic ground vehicle. The multirotor is modeled with nonlinear aerodynamic drag and collects measurements of the ground vehicle in the body reference frame each time step. Measurements of the target are also corrupted with random Gaussian noise that is zero mean and has a standard deviation of magnitude $\frac{1}{10}$. The ground vehicle uses a bicycle steering model, has variable elevation, and follows a cycled list of four waypoints that form the shape of a square about the inertial origin.

The ground vehicle also moves with a constant forward velocity of one meter per second, while the multirotor orbits with a velocity saturated at five meters per second and is commanded to face the ground vehicle at all times. We assume that a visual-inertial estimator is properly operating onboard the multirotor, providing the true linear and angular velocities, true IMU biases, as well as the true roll and pitch of the aircraft. The desired relative radius and altitude is set to five meters in all experiments.

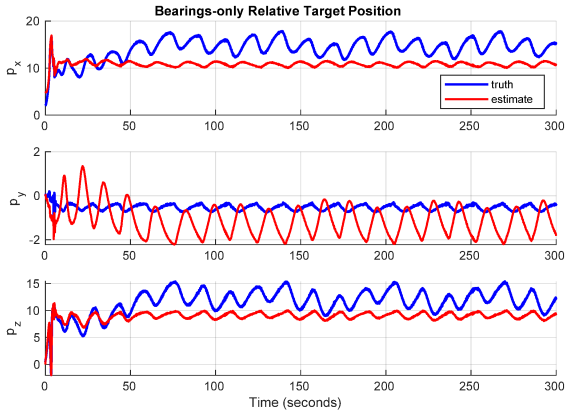

Fig. 1. Relative target position estimation over a one minute flight using the bearing-only observer defined in (7).

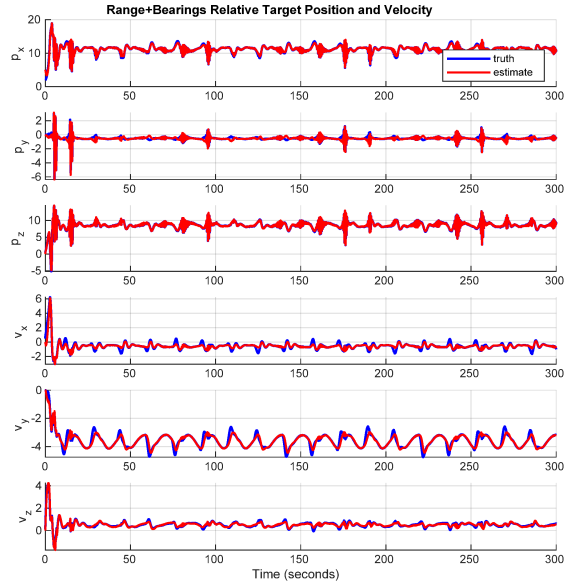

Fig. 2. Relative target position and velocity estimation over a one minute flight using the range with bearing observer defined in (16) and (17).

Figure 1 shows relative target position estimation using bearing-only measurements, while Figure 2 shows relative position and velocity estimates using range with bearing measurements. We see that flying at five times the velocity of the ground vehicle, the multirotor is able to correctly estimate the ground vehicles relative position using the range with bearing method and converges to a bounded region for the bearing-only method. However, about every 15 seconds, we observe larger deviations from truth, which is due to the sharp turns of the ground vehicle as it moves on to the next desired waypoint. This happens to both observers because neither one accounts for turns in their motion models, but because the turns are brief, the observers' estimates do not significantly deviate from truth.

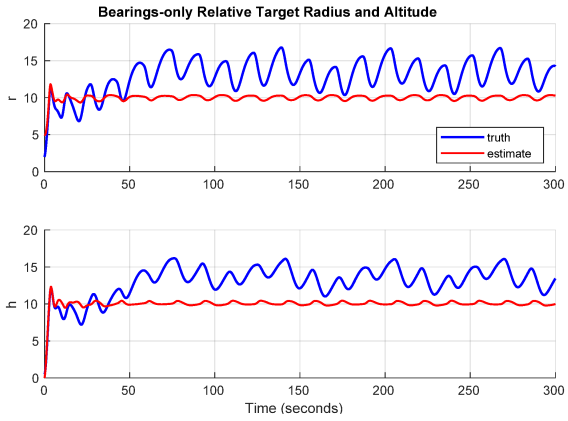

Fig. 3. Relative target radius and altitude over a one minute flight using the bearing-only observer defined in (7).

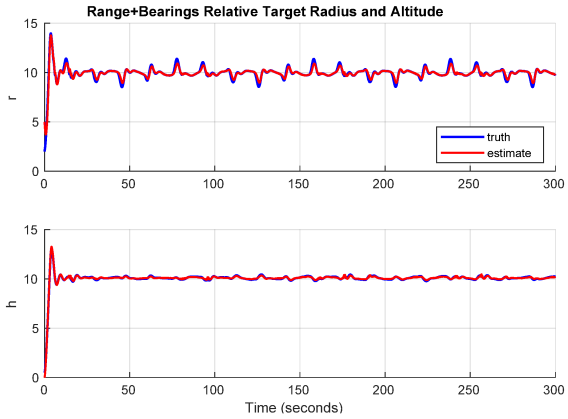

Fig. 4. Relative target radius and altitude estimation over a one minute flight using the range with bearing observer defined in (16) and (17).

Figures 3 and 4 show each observer's relative radius and altitude estimates over a one minute flight. The estimates quickly converge to the truth at the beginning of the simulation and experience larger deviations during sharp turns of the ground vehicle because that is where the observers' estimates experience a more significant deviation from truth. The velocity controller successfully drives the aircraft to the desired relative radius and altitude according to target estimation estimates, but we see that the true relative radius and altitude using the bearing-only observer deviates to a bounded region due to observer error.

Finally, Figures 5 and 6 depict the multirotor's commanded velocity versus its true velocity for both the bearing-only and range with bearing observers. The sensor noise applied to the measurements bleeds through into the commanded velocity most notably along the x axis, but we see

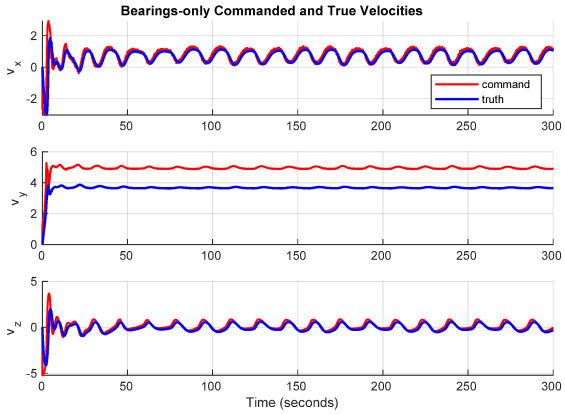

Fig. 5. Commanded versus true multirotor velocity over a one minute flight using the bearing-only observer defined in (7).

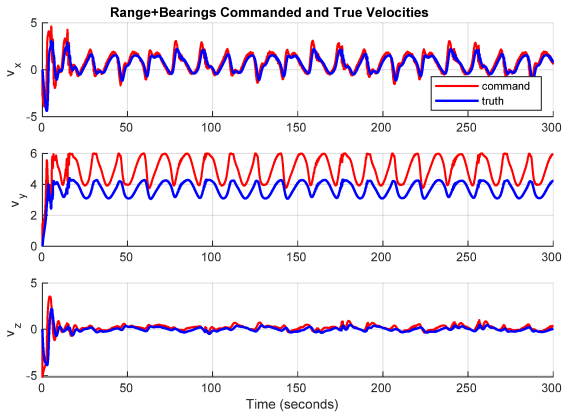

Fig. 6. Commanded versus true multirotor velocity over a one minute flight using the range with bearing observer defined in (16) and (17).

that the true velocity generally lines up with the commanded velocity throughout the flight with the exception of the y axis. This is primarily due to multirotor drag not being modeled in the derivation of the multirotor velocity controller, as we see a mostly constant offset between commanded velocity and true velocity.

VI. Conclusions and Future Work

We have developed nonlinear observers for relative target position and velocity estimation using bearing-only and range with bearing measurements. We also designed a controller to bring a multirotor aircraft to some desired body-level frame velocity and computed the velocity command that puts the aircraft into a circumnavigating orbit about the target. We have also shown mathematically and through simulation that a multirotor does indeed approach the desired relative radius and altitude using our controller and observers. This work has better enabled GPS-denied target tracking and circumnavigation from a multirotor aerial platform. Future work includes applications to fixed-wing aircraft, a hardware implementation of the observers and controller, development of a decision process during loss of target tracking, exploration of observers that account for higher order motion, and possibly accounting for aerodynamic drag and wind in the multirotor controller.

References

[1] R. Li, Y. Shi, and Y. Song, "Localization and circumnavigation of multiple agents along an unknown target based on bearing-only measurement: A three dimensional solution," *Automatica*, vol. 94, pp. 18–25, 2018.

[2] J. Ghommam, N. Fethalla, and M. Saad, "Quadrotor circumnavigation of an unknown moving target using camera vision-based measurements," *IET Control Theory & Applications*, vol. 10, no. 15, pp. 1874–1887, 2016.

[3] R. Mebarki, V. Lippiello, and B. Siciliano, "Nonlinear visual control of unmanned aerial vehicles in gps-denied environments," *IEEE Transactions on Robotics*, vol. 31, no. 4, pp. 1004–1017, 2015.

[4] M. Deghat, L. Xia, B. D. Anderson, and Y. Hong, "Multi-target localization and circumnavigation by a single agent using bearing measurements," *International Journal of Robust and Nonlinear Control*, vol. 25, no. 14, pp. 2362–2374, 2015.

[5] M. Deghat, I. Shames, B. D. Anderson, and C. Yu, "Localization and circumnavigation of a slowly moving target using bearing measurements," *IEEE Transactions on Automatic Control*, vol. 59, no. 8, pp. 2182–2188, 2014.

[6] Y. Cao, J. Muse, D. Casbeer, and D. Kingston, "Circumnavigation of an unknown target using uavs with range and range rate measurements," in *Decision and Control (CDC), 2013 IEEE 52nd Annual Conference on*. IEEE, 2013, pp. 3617–3622.

[7] M. Oispuu and J. Hörst, "Azimuth-only localization and accuracy study for piecewise curvilinearly moving targets," in *Information Fusion (FUSION), 2010 13th Conference on*. IEEE, 2010, pp. 1–8.

[8] R. Mur-Artal and J. D. Tardós, "ORB-SLAM2: An open-source SLAM system for monocular, stereo, and RGB-D cameras," *IEEE Transactions on Robotics*, vol. 33, no. 5, pp. 1255–1262, 2017.

[9] C. Forster, Z. Zhang, M. Gassner, M. Werlberger, and D. Scaramuzza, "SVO: Semidirect visual odometry for monocular and multicamera systems," *IEEE Transactions on Robotics*, vol. 33, no. 2, pp. 249–265, 2017.

[10] M. Bloesch, S. Omari, M. Hutter, and R. Siegwart, "Robust visual inertial odometry using a direct EKF-based approach," in *Intelligent Robots and Systems (IROS), 2015 IEEE/RSJ International Conference on*. IEEE, 2015, pp. 298–304.

[11] J. J. Tarrio and S. Pedre, "Realtime edge based visual inertial odometry for mav teleoperation in indoor environments," *Journal of Intelligent & Robotic Systems*, vol. 90, no. 1-2, pp. 235–252, 2018.

[12] R. Mahony and T. Hamel, "A geometric nonlinear observer for simultaneous localisation and mapping," in *Decision and Control (CDC), 2017 IEEE 56th Annual Conference on*. IEEE, 2017, pp. 2408–2415.

[13] K. Wu, T. Zhang, D. Su, S. Huang, and G. Dissanayake, "An invariant-ekf vins algorithm for improving consistency," in *Intelligent Robots and Systems (IROS), 2017 IEEE/RSJ International Conference on*. IEEE, 2017, pp. 1578–1585.

[14] D. O. Wheeler, D. P. Koch, J. S. Jackson, T. W. McLain, and R. W. Beard, "Relative navigation: A keyframe-based approach for observable gps-degraded navigation," *IEEE Control Systems Magazine*, vol. 38, no. 4, pp. 30–48, 2018.

[15] Y. Watanabe, P. Fabiani, and G. Le Besnerais, "Simultaneous visual target tracking and navigation in a gps-denied environment," in *Advanced Robotics, 2009. ICAR 2009. International Conference on*. IEEE, 2009, pp. 1–6.

[16] J. Pestana, J. L. Sanchez-Lopez, S. Saripalli, and P. Campoy, "Computer vision based general object following for gps-denied multirotor unmanned vehicles," in *American Control Conference (ACC), 2014*. IEEE, 2014, pp. 1886–1891.

[17] J. Nielsen and R. W. Beard, "Relative target estimation using a cascade of extended Kalman filters," in *Proceedings of the 30th International Technical Meeting of The Satellite Division of the Institute of Navigation (ION GNSS+ 2017)*, Portland, Oregon, September 2017, pp. 2273–2289.

[18] A. Martinelli, "Visual-inertial structure from motion: Observability and resolvability," in *Intelligent Robots and Systems (IROS), 2013 IEEE/RSJ International Conference on*. IEEE, 2013, pp. 4235–4242.